Developing a Thermal- and Coking-Resistant Cobalt-Tungsten Bimetallic Anode Catalyst for Solid Oxide Fuel Cells

Yan, N.; Pandey, J.; Zeng, Y.; Amirkhiz, B.S.; Hua, B.; Geels, N.J.; Luo, J.L.; Rothenberg, G.

DOI
10.1021/acscatal.6b01197

Publication date
2016

Document Version
Final published version

Published in
ACS Catalysis

ACS Catalysis

Letter

pubs.acs.org/acscatalysis

Developing a Thermal- and Coking-Resistant Cobalt–Tungsten Bimetallic Anode Catalyst for Solid Oxide Fuel Cells

Ning Yan,*[,†] Jay Pandey,[†] Yimin Zeng,[§] Babak S. Amirkhiz,[§] Bin Hua,[‡] Norbert J. Geels,[†] Jing-Li Luo,[‡] and Gadi Rothenberg[†]

[†]Van't Hoff Institute for Molecular Sciences (HIMS), University of Amsterdam, Amsterdam, 1098XH, The Netherlands

[‡]Department of Chemical and Materials Engineering, University of Alberta, Edmonton, Alberta T6G 1H9, Canada

[§]CanmetMATERIALS, Natural Resources Canada, Hamilton, Ontario L8P 0A5, Canada

Supporting Information

ABSTRACT: We report the development of a novel Co–W bimetallic anode catalyst for solid oxide fuel cells (SOFCs) via a facile infiltration-annealing process. Using various microscopic and spectroscopic measurements, we find that the formed intermetallic nanoparticles are highly thermally stable up to 900 °C and show good coking resistance in methane. In particular, a fuel cell fitted with Co_3W anode shows comparable activity (relative to Co) in the electro-oxidation of hydrogen and methane at 900 °C without suffering significant degradation during a longevity test.

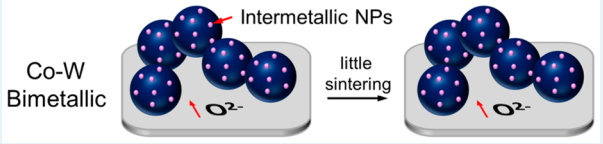

KEYWORDS: *nanoparticle, intermetallic compound, thermal stability, high temperature fuel cells, carbon resistance*

In the global quest for efficient energy conversion, solid oxide fuel cells (SOFCs) are receiving more and more attention for decades, because of their higher fuel flexibility and efficiency.[1−8] Indeed, their elevated operation temperature (600−800 °C) grants various advantages, such as improved electrokinetics and better overall thermal efficiency. However, this inevitably generates concerns regarding the thermal stability of the electrocatalyst, particularly when nanosized active species are used.[9−15] In fact, metallic nanoelectrocatalysts are widely used as the anode component of SOFCs, offering improved fuel oxidation activity. Such well-dispersed nanoparticles expand the triple-phase boundary areas, demonstrate higher redox stability, and even resist coke formations.[10,11,16] Unfortunately, these catalysts suffer from severe sintering problems, via either migration−coalescence or Ostwald ripening pathways.[17] The inherent poor thermal stability remains a major challenge of their practical implementation.

Although organic capping agents, which are the commonly used stabilizers of nanoparticles, are not suitable for applications at temperatures of >400 °C,[18−21] recent studies have shown promising alternative approaches for mitigating particle growth. These include (i) encapsulation of the catalytically active metal nanoparticle using a thin shell of oxides;[22−25] (ii) the improvement of the metal−support interaction energy,[16,26−30] e.g., via "socketing" nano species in the host oxides; and (iii) control of the three-dimensional (3-D) distribution of metal particles, achieving optimized interparticle spacings.[31−33] However, the complex preparation protocols make these catalysts too costly for large-scale applications.

Another approach for increasing temperature stability is by preparing a bimetallic nanocatalyst[34−38] that contains a higher-melting-point alloying element. This approach is restricted to specific chemical compositions, yet such alloys can enable the "best of two worlds", combining superior activity with high stability, as well as improved price/performance ratios.[39] In theory, this could open a route to active and stable fuel cell anodes. Specifically, the structurally ordered intermetallic compound has a well-defined composition and lattice structure, providing predictable control over various catalytic properties. Many of these catalysts have shown excellent electrochemical activity in fuel cell applications.[40−44]

Here, we report the synthesis of CoW bimetallic nanoparticle alloys and their application as SOFC anode catalysts. The optimized alloys exhibit exceptional thermal stability up to 900 °C, excellent electrochemical activity, and good coking resistance. We believe that this generic approach toward developing "self-stabilized" nanosized catalysts opens exciting opportunities for a variety of high-temperature catalytic processes.

We prepared catalyst samples with three compositions—Co, Co_3W, and CoW—by infiltrating stoichiometric amounts of $Co(NO_3)_2{\cdot}6H_2O$ and $(NH_4)_{10}W_{12}O_{41}{\cdot}5H_2O$ onto the substrates, followed by calcination at 800 °C and annealing in hydrogen at 900 °C (see the Supporting Information for details). Figures 1a−e, as well as Figure S1, show the high-angle annular dark field (HAADF) image of 10 wt % Co_3W on yttria-stabilized zirconia (YSZ) and the corresponding elemental mappings using energy-dispersive X-ray spectroscopy (EDX). Co and W formed bimetallic particles, yet no monometallic

Received: April 28, 2016
Revised: June 12, 2016
Published: June 14, 2016

DOI: 10.1021/acscatal.6b01197
ACS Catal. 2016, 6, 4630−4634

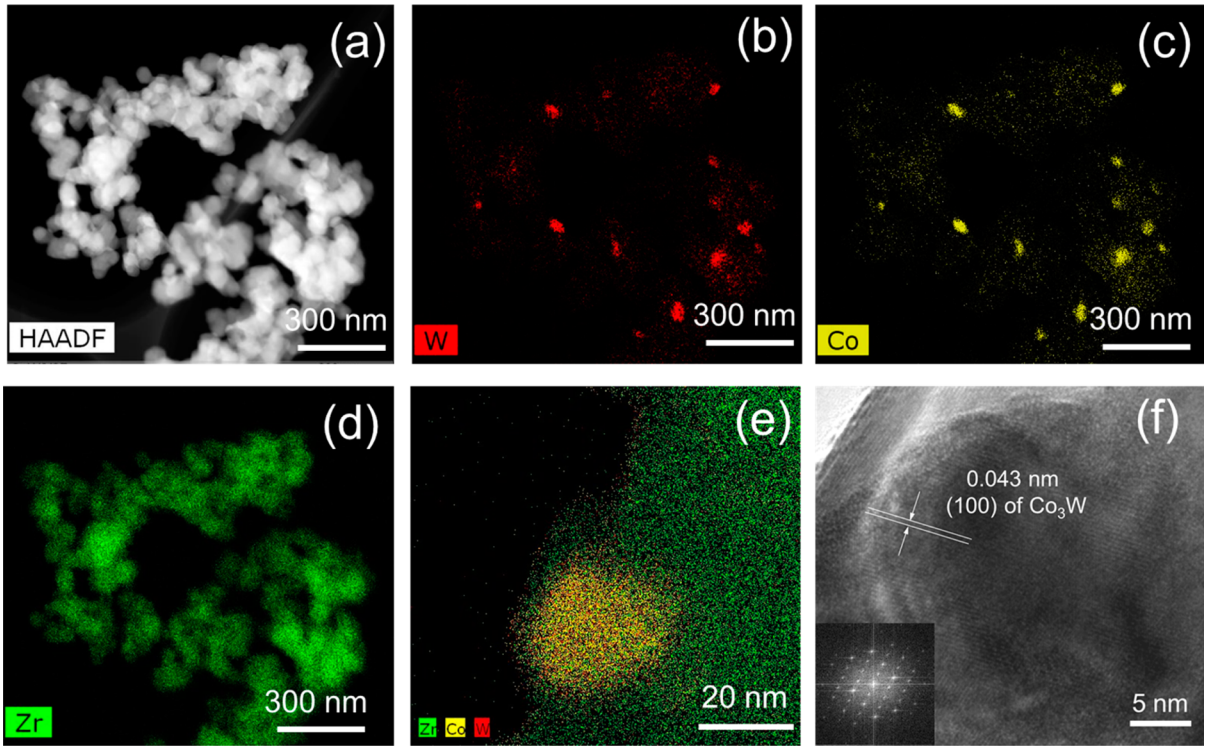

Figure 1. (a) TEM-HAADF image of a Co_3W bimetallic catalyst supported on YSZ and the corresponding EDX elemental mappings of (b) W (in red), (c) Co (in yellow), (d) Zr (in green), and (e) overlaid Co, W, and Zr for a single nanoparticle; (f) HRTEM micrograph of the Co_3W nanoparticle shown in panel (e).

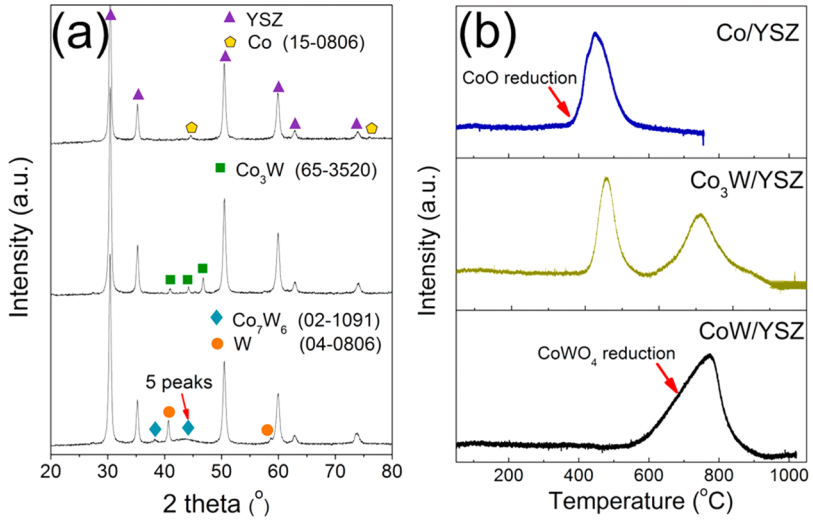

Figure 2. (a) XRD patterns of YSZ supported Co, Co_3W, and CoW catalysts; the number shown in the bracket indicates the JPCDS file number. (b) Temperature-programmed reduction in hydrogen gas (H_2-TPR) spectra of the catalyst precursors.

particles were identified. This shows the effectiveness of preparing alloys via this facile infiltration-annealing approach. The bimetallic nanoparticles, 10−50 nm in size, remained well-distributed over the YSZ, even after 24 h of annealing at 900 °C, implying an exceptional thermal stability for Co_3W (see below). Examination of the high-resolution transmission electron microscopy (HRTEM) micrograph, as well as the diffraction pattern in Figure 1f, suggests that this nanoparticle had a Co_3W intermetallic crystallographic phase, showing the (100) facet of Co_3W. Morphological characterizations regarding CoW can be found in the Supporting Information (Figures S2 and S3). An additional core−shell structure, Co_7W_6@W, was identified on the YSZ surface. Their dispersion also demonstrated high homogeneity, with a typical dimension of ∼30 nm.

X-ray diffraction (XRD) studies also offered evidence for the formation of the intermetallic phases. Looking at the XRD patterns in Figure 2a, we see that Co_3W intermetallic compound (Joint Committee on Powder Diffraction Standards (JCPDS) File No. 65-3520) was produced in the Co_3W sample, whereas a mixture of metallic W and intermetallic Co_7W_6 (JPCDS File No. 02-1091) formed in the CoW group. These observations were in good agreement with the TEM data and the prediction of the thermodynamic phase diagram.[45] In these

DOI: 10.1021/acscatal.6b01197
ACS Catal. 2016, 6, 4630−4634

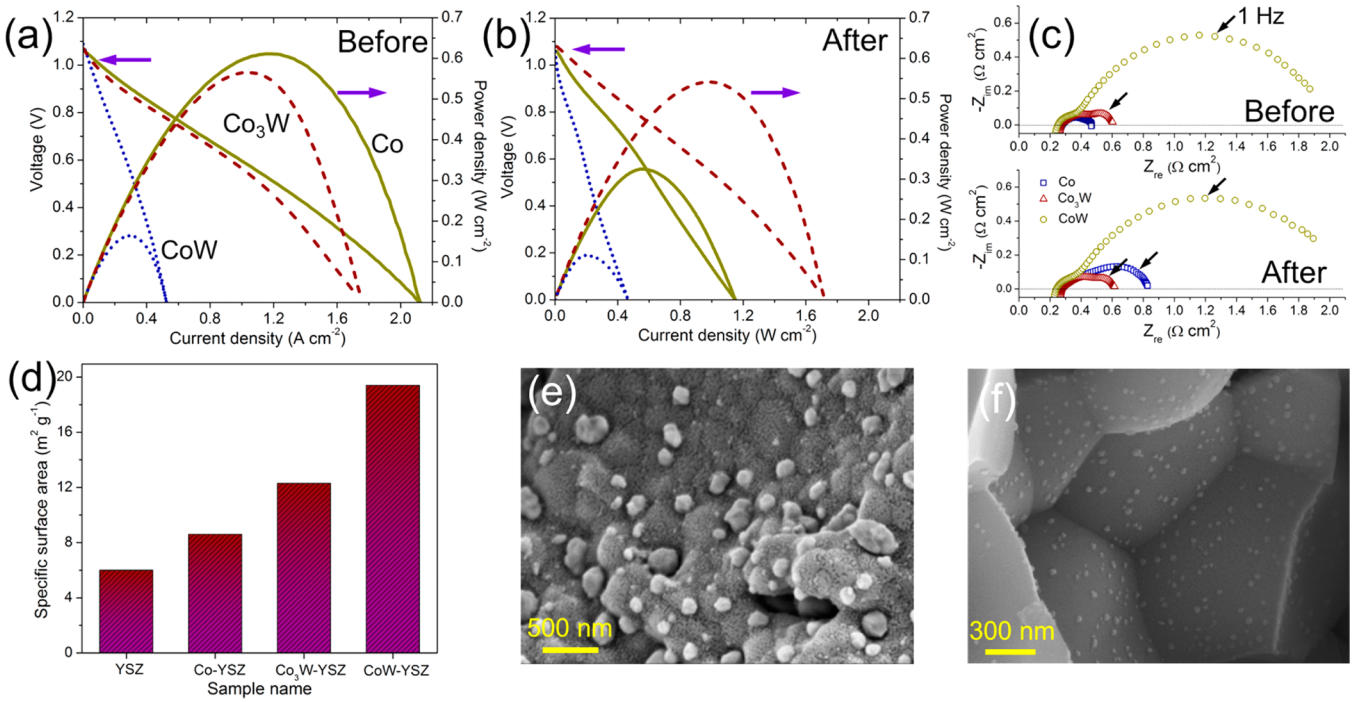

Figure 3. (a, b) Polarization and power density plots of Co (solid line), Co_3W (dashed line), and CoW (dotted line) cells at 900 °C before (panel (a)) and after (panel (b)) 24 h of heat treatment and (c) the corresponding impedance spectra obtained in H_2 at 900 °C before and after 24 h of heat treatment; (d) the BET surface area data of YSZ-supported catalyst after 24 h of thermal treatment in H_2; (e) Co-infiltrated YSZ electrode scaffold after 0.5 h of annealing in H_2 at 900 °C; and (f) Co_3W-infiltrated YSZ electrode scaffold after 0.5 h of annealing in H_2 at 900 °C.

intermetallic compounds (Co_3W and Co_7W_6), the metallic bondings remain, offering a unique compromise between ceramic and metallic properties. Thus, this type of alloy has both a high melting point (similar to a ceramic) and excellent electronic conductivity (similar to a metal). These two features are the critical ones for a good high-temperature electrocatalyst.

The temperature-programmed reduction in hydrogen gas (H_2-TPR) analysis reveals how these intermetallics were formed (see Figure 2b). The two peaks of calcined Co_3W precursor corresponded to the reductions of CoO (ca. 475 °C) and $CoWO_4$ (ca. 800 °C), sequentially forming Co_3W intermetallic after annealing. Supporting XRD data regarding the formation of $CoWO_4$ intermediate can be found in Figure S4a in the Supporting Information. The single peak of CoW precursor could be ascribed to the reduction of $CoWO_4$ that then yielded Co_7W_6 and W. Besides, the Fourier transform infrared (FTIR) spectra in Figure S5 in the Supporting Information indicate that all tungsten species have been fully reduced. The transmittance peak at 840 cm^{-1}, relating to the stretching mode of the W═O bond in the tungsten oxide species,[46] in the bimetallic precursor disappeared completely after the designated annealing in H_2.

The electrochemical performances of these anode catalysts were tested in the electrolyte-supported SOFC, consisting of a $La_{0.6}Sr_{0.4}Co_{0.2}Fe_{0.8}O_3$ (LSCF)-infiltrated cathode, a thick YSZ electrolyte, and a $La_{0.4}Sr_{0.6}TiO_3$(LST)-infiltrated anode containing ∼5 wt % of the examined catalyst (see the Supporting Information for the detailed preparation protocol of the membrane electrode assembly and Figure S6 in the Supporting Information for a schematic drawing of the electrode). The XRD pattern in Figure S4b confirmed that the infiltrated LST and Co_3W had excellent chemical compatibility. Initially, both Co and Co_3W anode showed good activities toward H_2 electrochemical oxidation at 900 °C, achieving maximum power densities of 0.61 W cm^{-2} and 0.57 W cm^{-2}, respectively (see Figure 3a). The intermetallic catalyst itself might be highly active, or the excellent activity might be attributable to the segregation of Co atoms on the surface, as observed in previous research.[42] In contrast, the maximum power density of CoW was merely 0.17 W cm^{-2}, presumably pertaining to the tungsten shells formed on the CoW nanoparticles, which were proven to be catalytically inactive (see the TEM micrographs in Figure S3 in the Supporting Information).[47]

To evaluate the stability of the catalysts, the same cells were maintained at 900 °C in H_2 for a 24 h isothermal treatment before further measurements. We then saw that the control Co cell degraded dramatically, with a maximum power density of 0.33 W cm^{-2} (Figure 3b). Moreover, the area-specific polarization resistance increased from 0.47 Ω cm^2 to 0.83 Ω cm^2 (Figure 3c; note that the ohmic resistance varied only slightly). The fitted impedance spectra and the equivalent circuit are shown in Figure S7 in the Supporting Information.[48,49] However, the excellent catalytic behavior of Co_3W was maintained, with a power density drop of <10%. The high stability of the infiltrated LSCF cathode and the LST anode were reported elsewhere.[50,51] Thus, we maintain that the thermal stability of the metallic infiltrates is the key factor governing the long-term robustness of the specific cell (cf. the highly dispersive Co_3W nanoparticles observed in Figure 1 after 24 h of annealing in H_2).

This conclusion was further supported by the Brunauer–Emmett–Teller (BET) specific surface area analysis and by scanning electron microscopy (SEM) of the heat-treated samples. Figure 3d compares the specific surface areas of four powder catalysts. The loading of the metallic species did increase the surface areas of YSZ, because of the presence of the impregnated nanoparticles. Relative to Co catalyst, this effect was much more prominent for bimetallic samples, suggesting

DOI: 10.1021/acscatal.6b01197
ACS Catal. 2016, 6, 4630–4634

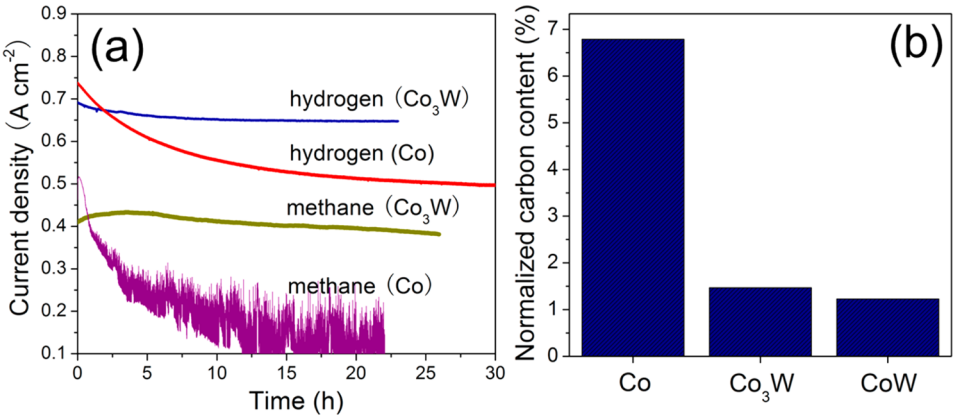

Figure 4. (a) Potentiostatic tests at 0.7 V of Co and Co_3W cells in the streams of hydrogen or methane at 900 °C; (b) carbon deposition measurements for various YSZ supported catalysts after 5 h exposure to methane feedstream at 800 °C.

that smaller Co_3W and CoW infiltrates were sustained after the 24 h heat treatment. The SEM images in Figures 3e and 3f confirm the exceptional thermal stability of Co_3W. For clearer observations, the nanoparticles were infiltrated directly into the plain porous YSZ scaffold without preloading LST as the electronic conductor. After only 0.5 h of annealing at 900 °C in H_2, the Co nanoparticles coalesced substantially, forming big clusters ranging from 100 nm to 300 nm in size on the YSZ surface. This sintering effect of Co nanoparticles is well-documented.[52,53] Conversely, the fine Co_3W nanostructure was not destructed by the heat treatment; the particle size remained <50 nm. Figure S8 in the Supporting Information shows a schematic comparison of the sintering resistances of these two nanoparticles.

Excitingly, the Co_3W catalyst also showed good coking resistance during a longevity test. Figure 4a shows the potentiostatic test under a constant voltage load of 0.7 V in a stream of methane. Only a trace of degradation was seen after more than 25 h. The corresponding polarization curves of the Co_3W cell in methane before and after this stability test are shown in Figure S9 in the Supporting Information (similarly, the comparison under OCV conditions was also shown). The slight degradation, particularly in the low potential region, might be mainly due to the sintering effect. Although methane decomposition is thermodynamically favorable at 900 °C, the carbon deposition in Co_3W cells was greatly suppressed, compared with the Co cell (see Figure S10 in the Supporting Information). Though carbon filament formation was observed that led to the decreased performances in Figure S9, the majority of Co_3W particles remained free of carbon deposits. Note that the Co cell degraded rapidly in methane, as a result of combined sintering and coking effects. In addition, the discharging test also compares the electrochemical stability of the Co and Co_3W cells in H_2, in which the Co_3W cell showed negligible degradation after the 24 h test. The semiquantitative coking resistance measurement was performed using thermogravimetric analysis (TGA) before which the examined catalysts were subjected to a 5 h exposure to methane at 800 °C. Notably, the carbon deposits in Co/YSZ reached almost 7 wt % (see Figure 4b). This is not surprising, as cobalt nanoparticles are reported to be extremely active, catalyzing the methane conversion to carbon filaments/nanotubes.[54,55] For both the Co_3W and the CoW bimetallic catalyst, the carbon contents were insignificant, demonstrating great potential for uses in hydrocarbon fuels. The decoking mechanism might involve the formation of tungstic acid on the alloy surface (see Figure S3). This acid was reported to suppress carbon deposition in methane,[56,57]

In conclusion, we have discovered that Co_3W nanoparticle alloys are excellent SOFC anode catalysts, with exceptional thermal stability and high activity. More generally, the facile "self-stabilizing" synthesis strategy reported here opens opportunities for the designing new catalysts for SOFCs and other high-temperature applications.

■ ASSOCIATED CONTENT

Supporting Information

The Supporting Information is available free of charge on the ACS Publications website at DOI: 10.1021/acscatal.6b01197.

Experimental details and additional characterization data (TEM, XRD, FTIR, SEM, and electrochemical tests) (PDF)

■ AUTHOR INFORMATION

Corresponding Author

*E-mail: n.yan@uva.nl.

Notes

The authors declare no competing financial interest.

■ ACKNOWLEDGMENTS

We thank the Natural Sciences and Engineering Research Council of Canada (NSERC) and the Resource for the Innovation of Engineered Materials (RIEM) program of CanmetMATERIALS, Natural Resources Canada for financial support. This work is part of the Research Priority Area Sustainable Chemistry of the UvA (http://suschem.uva.nl).

■ REFERENCES

(1) Tao, S. W.; Irvine, J. T. S. *Nat. Mater.* **2003**, *2*, 320−323.
(2) McIntosh, S.; Gorte, R. J. *Chem. Rev.* **2004**, *104*, 4845−4865.
(3) Yang, L.; Wang, S.; Blinn, K.; Liu, M.; Liu, Z.; Cheng, Z.; Liu, M. *Science* **2009**, *326*, 126−129.
(4) Guzman, F.; Singh, R.; Chuang, S. S. C. *Energy Fuels* **2011**, *25*, 2179−2186.
(5) Yan, N.; Fu, X.-Z.; Luo, J.-L.; Chuang, K. T.; Sanger, A. R. *J. Power Sources* **2012**, *198*, 164−169.
(6) Yan, N.; Luo, J.-L.; Chuang, K. T. *J. Power Sources* **2014**, *250*, 212−219.
(7) Garcia, A.; Yan, N.; Vincent, A.; Singh, A.; Hill, J. M.; Chuang, K. T.; Luo, J.-L. *J. Mater. Chem. A* **2015**, *3*, 23973−23980.

DOI: 10.1021/acscatal.6b01197
ACS Catal. 2016, 6, 4630−4634

(8) Jiang, S. P.; Chan, S. H. *J. Mater. Sci.* **2004**, *39*, 4405−4439.
(9) Adijanto, L.; Sampath, A.; Yu, A. S.; Cargnello, M.; Fornasiero, P.; Gorte, R. J.; Vohs, J. M. *ACS Catal.* **2013**, *3*, 1801−1809.
(10) Stefan, E.; Tsekouras, G.; Irvine, J. T. S. *Adv. Energy Mater.* **2013**, *3*, 1454−1462.
(11) Xiao, G.; Wang, S.; Lin, Y.; Zhang, Y.; An, K.; Chen, F. *ACS Appl. Mater. Interfaces* **2014**, *6*, 19990−19996.
(12) Yang, G. M.; Su, C.; Chen, Y. B.; Tade, M. O.; Shao, Z. P. *J. Mater. Chem. A* **2014**, *2*, 19526−19535.
(13) Zhang, L.; Yang, C. H.; Frenkel, A. I.; Wang, S. W.; Xiao, G. L.; Brinkman, K.; Chen, F. L. *J. Power Sources* **2014**, *262*, 421−428.
(14) Tong, X. F.; Luo, T.; Meng, X.; Wu, H.; Li, J. L.; Liu, X. J.; Ji, X. N.; Wang, J. Q.; Chen, C. S.; Zhan, Z. L. *Small* **2015**, *11*, 5581−5588.
(15) Hua, B.; Yan, N.; Li, M.; Zhang, Y.-q.; Sun, Y.-f.; Li, J.; Etsell, T.; Sarkar, P.; Chuang, K.; Luo, J.-L. *Energy Environ. Sci.* **2016**, *9*, 207−215.
(16) Neagu, D.; Oh, T.-S.; Miller, D. N.; Menard, H.; Bukhari, S. M.; Gamble, S. R.; Gorte, R. J.; Vohs, J. M.; Irvine, J. T. S. *Nat. Commun.* **2015**, *6*, 8120.
(17) Hansen, T. W.; Delariva, A. T.; Challa, S. R.; Datye, A. K. *Acc. Chem. Res.* **2013**, *46*, 1720−1730.
(18) Ott, L. S.; Finke, R. G. *Coord. Chem. Rev.* **2007**, *251*, 1075−1100.
(19) Kuhn, J. N.; Tsung, C.-K.; Huang, W.; Somorjai, G. A. *J. Catal.* **2009**, *265*, 209−215.
(20) Ferry, A.; Schaepe, K.; Tegeder, P.; Richter, C.; Chepiga, K. M.; Ravoo, B. J.; Glorius, F. *ACS Catal.* **2015**, *5*, 5414−5420.
(21) Pavlovic, M.; Adok-Sipiczki, M.; Horvath, E.; Szabo, T.; Forro, L.; Szilagyi, I. *J. Phys. Chem. C* **2015**, *119*, 24919−24926.
(22) Arnal, P. M.; Comotti, M.; Schueth, F. *Angew. Chem., Int. Ed.* **2006**, *45*, 8224−8227.
(23) Qiao, Z. A.; Zhang, P. F.; Chai, S. H.; Chi, M. F.; Veith, G. M.; Gallego, N. C.; Kidder, M.; Dai, S. *J. Am. Chem. Soc.* **2014**, *136*, 11260−11263.
(24) Li, S. W.; Tuel, A.; Meunier, F.; Aouine, M.; Farrusseng, D. *J. Catal.* **2015**, *332*, 25−30.
(25) Wang, X.; Liu, D.; Li, J.; Zhen, J.; Wang, F.; Zhang, H. *Chem. Sci.* **2015**, *6*, 2877−2884.
(26) Farmer, J. A.; Campbell, C. T. *Science* **2010**, *329*, 933−936.
(27) Liu, Y.; Liu, B.; Liu, Y.; Wang, Q.; Hu, W.; Jing, P.; Liu, L.; Yu, S.; Zhang, J. *Appl. Catal., B* **2013**, *142−143*, 615−625.
(28) Zhang, G.; Sun, T.; Peng, J.; Wang, S.; Wang, S. *Appl. Catal., A* **2013**, *462−463*, 75−81.
(29) Zhang, B. S.; Shao, L. D.; Zhang, W.; Sun, X. Y.; Pan, X. L.; Su, D. S. *ChemCatChem* **2014**, *6*, 2607−2612.
(30) Yoon, D. Y.; Kim, Y. J.; Lim, J. H.; Cho, B. K.; Hong, S. B.; Nam, I.-S.; Choung, J. W. *J. Catal.* **2015**, *330*, 71−83.
(31) Prieto, G.; Zecevic, J.; Friedrich, H.; de Jong, K. P.; de Jongh, P. E. *Nat. Mater.* **2012**, *12*, 34−39.
(32) Plessers, E.; Stassen, I.; Sree, S. P.; Janssen, K. P. F.; Yuan, H. F.; Martens, J.; Hofkens, J.; De Vos, D.; Roeffaers, M. B. J. *ACS Catal.* **2015**, *5*, 6690−6695.
(33) Zecevic, J.; Vanbutsele, G.; de Jong, K. P.; Martens, J. A. *Nature* **2015**, *528*, 245−248.
(34) Dhakad, M.; Fino, D.; Rayalu, S. S.; Kumar, R.; Watanabe, A.; Haneda, H.; Devotta, S.; Mitsuhashi, T.; Labhsetwar, N. *Top. Catal.* **2007**, *42−43*, 273−276.
(35) Cao, A.; Veser, G. *Nat. Mater.* **2010**, *9*, 75−81.
(36) Calderone, V. R.; Shiju, N. R.; Ferre, D. C.; Rothenberg, G. *Green Chem.* **2011**, *13*, 1950−1959.
(37) Huang, R.; Wen, Y.-H.; Zhu, Z.-Z.; Sun, S.-G. *J. Phys. Chem. C* **2012**, *116*, 8664−8671.
(38) Han, C. W.; Majumdar, P.; Marinero, E. E.; Aguilar-Tapia, A.; Zanella, R.; Greeley, J.; Ortalan, V. *Nano Lett.* **2015**, *15*, 8141−8147.
(39) Calderone, V. R.; Shiju, N. R.; Curulla-Ferre, D.; Chambrey, S.; Khodakov, A.; Rose, A.; Thiessen, J.; Jess, A.; Rothenberg, G. *Angew. Chem., Int. Ed.* **2013**, *52*, 4397−4401.
(40) Matsumoto, F.; Roychowdhury, C.; DiSalvo, F. J.; Abruna, H. D. *J. Electrochem. Soc.* **2008**, *155*, B148−B154.
(41) Du, C.; Chen, M.; Wang, W.; Tan, Q.; Xiong, K.; Yin, G. *J. Power Sources* **2013**, *240*, 630−635.
(42) Wang, D.; Xin, H. L.; Hovden, R.; Wang, H.; Yu, Y.; Muller, D. A.; DiSalvo, F. J.; Abruna, H. D. *Nat. Mater.* **2012**, *12*, 81−87.
(43) Ramesh, G. V.; Kodiyath, R.; Tanabe, T.; Manikandan, M.; Fujita, T.; Matsumoto, F.; Ishihara, S.; Ueda, S.; Yamashita, Y.; Ariga, K.; Abe, H. *ChemElectroChem* **2014**, *1*, 728−732.
(44) Sanetuntikul, J.; Ketpang, K.; Shanmugam, S. *ACS Catal.* **2015**, *5*, 7321−7327.
(45) Okamoto, H. *J. Phase Equilib. Diffus.* **2008**, *29*, 119−119.
(46) Yu, X. F.; Wu, N. Z.; Huang, H. Z.; Xie, Y. C.; Tang, Y. Q. *J. Mater. Chem.* **2001**, *11*, 3337−3342.
(47) Torabi, A.; Etsell, T. H. *J. Power Sources* **2012**, *212*, 47−56.
(48) Jiang, S. P.; Love, J. G.; Ramprakash, Y. *J. Power Sources* **2002**, *110*, 201−208.
(49) Hauch, A.; Ebbesen, S. D.; Jensen, S. H.; Mogensen, M. *J. Electrochem. Soc.* **2008**, *155*, B1184−B1193.
(50) Afshar, M. R.; Yan, N.; Zahiri, B.; Mitlin, D.; Chuang, K. T.; Luo, J.-L. *J. Power Sources* **2015**, *274*, 211−218.
(51) Roushanafshar, M.; Yan, N.; Chuang, K. T.; Luo, J.-L. *Appl. Catal., B* **2015**, *176-177*, 627−636.
(52) Saib, A. M.; Moodley, D. J.; Ciobica, I. M.; Hauman, M. M.; Sigwebela, B. H.; Weststrate, C. J.; Niemantsverdriet, J. W.; van de Loosdrecht, J. *Catal. Today* **2010**, *154*, 271−282.
(53) Eschemann, T. O.; de Jong, K. P. *ACS Catal.* **2015**, *5*, 3181−3188.
(54) Nemes, T.; Chambers, A.; Baker, R. T. K. *J. Phys. Chem. B* **1998**, *102*, 6323−6330.
(55) Huh, Y.; Green, M. L. H.; Kim, Y. H.; Lee, J. Y.; Lee, C. J. *Appl. Surf. Sci.* **2005**, *249*, 145−150.
(56) Yoon, D.; Manthiram, A. *Energy Environ. Sci.* **2014**, *7*, 3069−3076.
(57) Zhang, S.; Shi, C.; Chen, B.; Zhang, Y.; Qiu, J. *Catal. Commun.* **2015**, *69*, 123−128.

DOI: 10.1021/acscatal.6b01197
ACS Catal. 2016, 6, 4630−4634